Published in Journal of Molecular Biology 302, issue 1, 135-154, 2000
which should be used for any reference to this work

Crystal Structures of Two Functionally Different Thioredoxins in Spinach Chloroplasts

Guido Capitani[1]*, Zora Marković-Housley[1], Gregoire DelVal[2] May Morris[2], Johan N. Jansonius[1] and Peter Schürmann[2]

[1]*Structural Biology Division Biozentrum, University of Basel, CH-4056, Basel Switzerland*

[2]*Laboratoire de Biochimie végétale, University of Neuchâtel, CH-2007, Neuchâtel Switzerland*

Thioredoxins are small ubiquitous proteins which act as general protein disulfide reductases in living cells. Chloroplasts contain two distinct thioredoxins (*f* and *m*) with different phylogenetic origin. Both act as enzyme regulatory proteins but have different specificities towards target enzymes. Thioredoxin *f* (Trx f), which shares only low sequence identity with thioredoxin *m* (Trx m) and with all other known thioredoxins, activates enzymes of the Calvin cycle and other photosynthetic processes. Trx m shows high sequence similarity with bacterial thioredoxins and activates other chloroplast enzymes. The here described structural studies of the two chloroplast thioredoxins were carried out in order to gain insight into the structure/function relationships of these proteins. Crystal structures were determined for oxidized, recombinant thioredoxin *f* (Trx f-L) and at the N terminus truncated form of it (Trx f-S), as well as for oxidized and reduced thioredoxin *m* (at 2.1 and 2.3 Å resolution, respectively). Whereas thioredoxin *f* crystallized as a monomer, both truncated thioredoxin *f* and thioredoxin *m* crystallized as non-covalent dimers. The structures of thioredoxins *f* and *m* exhibit the typical thioredoxin fold consisting of a central twisted five-stranded β-sheet surrounded by four α-helices. Thioredoxin *f* contains an additional α-helix at the N terminus and an exposed third cysteine close to the active site. The overall three-dimensional structures of the two chloroplast thioredoxins are quite similar. However, the two proteins have a significantly different surface topology and charge distribution around the active site. An interesting feature which might significantly contribute to the specificity of thioredoxin *f* is an inherent flexibility of its active site, which has expressed itself crystallographically in two different crystal forms.

Keywords: spinach; chloroplast; thioredoxin *f*; thioredoxin *m*; X-ray structure

*Corresponding author

Introduction

Thioredoxins are small redox-active, very stable proteins which are found in all living cells (Holmgren, 1989, 1995). Their active site is characterized by a conserved disulfide-containing motif, -Trp-Cys-Gly-Pro-Cys- (Figure 1), which can undergo reversible oxidation-reduction. Thioredoxins reduce disulfide groups in many target proteins and thus take part in a vast spectrum of biological processes, from cell division and blood clotting to seed germination, insulin degradation and enzyme regulation. In oxygenic photosynthetic cells they act as important enzyme regulatory proteins (Buchanan *et al.*, 1994). For several years these functions have attracted considerable atten-

Present addresses: G. Capitani, Biochemisches Institut der Universität Zürich, Winterthurerstrasse 190, CH-8057 Zürich, Switzerland; G. DelVal, University of California at Berkeley, Department of Plant and Microbial Biology, 111 Koshland Hall, Berkeley, CA 94720-3102, USA.

Abbreviations used: Trx f, thiroedoxin f; Trx f-L, recombinant thioredoxin f; Trx f-S, N terminus truncated form of Trx f; Trx m, thioredoxin *m*; *E. coli* Trx, *E. coli* thioredoxin; human Trx, human thioredoxin; *Anabaena* Trx, thioredoxin 2 from *Anabaena sp.*, FBPase, fructose 1,6-bisphosphatase; NCS, non-crystallographic symmetry; SIRAS, single isomorphous replacement with anomalous scattering; MIRAS, multiple isomorphous replacement with anomalous scattering; wt, wild-type.

E-mail address of the corresponding author: capitani@biocfebs.unizh.ch

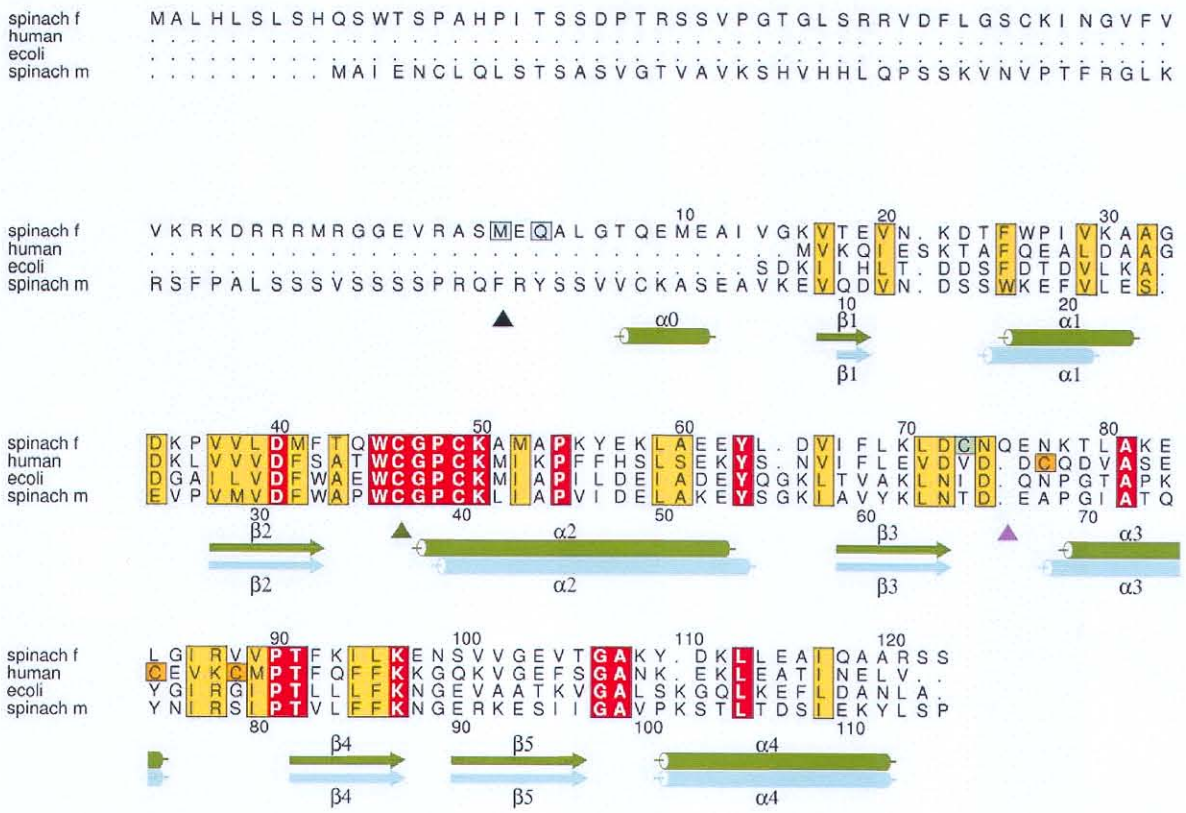

Figure 1. Structure-based multiple sequence aligment of four thioredoxin sequences from the SWISS-PROT (sw) database. The database codes are as follows. **Spinach f** sw:thif_spiol (precursor sequence; the two residues which differ in the wt purified Trx f from the recombinant enzyme used for crystallization are boxed in light cyan. The black triangle indicates the N terminus of the wt purified sequence). *E. coli:* sw:thio_ecoli. **Human:** sw:thio_human. **Spinach m:** sw:thim_spiol (precursor sequence). The residue numbering of Trx f is given on the top line and that of Trx m on the bottom line. The secondary structural elements of Trx f-L appear in green, those of Trx m (molecule B) in cyan. The secondary structure assignments for Trx m molecule A deviate slightly for helix α2, which encompasses residues 37 to 54, helix α4 (residues 100 to 112) and strand β5 (residues 90 to 97). Fully conserved residues are boxed in red, the ones which have a conservation level higher than 7 according to Livingstone & Barton (1993) appear in yellow. The exposed Cys46 (Trx f) is indicated by a green triangle. The third, accessible, cysteine residue in the Trx f sequence, Cys73, is boxed in light green, whereas the three additional cysteine residues of human thioredoxin are boxed in light orange. A magenta triangle pinpoints the Gln77 insertion in the Trx f sequence. The Figure was prepared with PROMOTIF and ALSCRIPT (Barton, 1993).

tion. Accordingly, a large amount of information is now available on this protein family and many amino acid sequences have been determined from a large variety of organisms. The active-site residues of all thioredoxins are highly conserved, but the remainder of the molecule can vary quite considerably in sequence.

Whereas in *Escherichia coli*, yeast, animal and human cells two types of functional thioredoxins have been reported, located in the cytoplasm and in the mitochondria of the eukaryotic organisms, plant cells contain two more, thioredoxin *f* and thioredoxin *m*, both present in the same cell compartment, the chloroplast (Jacquot *et al.*, 1997). The amino acid sequence of thioredoxin *f* (Trx f) shares only low identity with the other known sequences of the thioredoxin family, and even with the other chloroplastic thioredoxin, thioredoxin *m* (Trx m). It is remarkable that the sequence identity between Trx f and Trx m (29 %) is somewhat lower than the one between Trx f and mammalian thioredoxins (Eklund *et al.*, 1991) (around 30 %, with a maximum of 35 % in the case of human thioredoxin (human Trx)). These differences have functional consequences: Trx f can form a stable complex with, and very specifically, activate the chloroplastic fructose 1,6-bisphosphatase (FBPase), which participates in the Calvin cycle. Moreover, it is known to activate two further enzymes of the Calvin cycle, phosphoribulokinase and sedoheptulose bisphosphatase (Nishizawa & Buchanan, 1981), and, outside of the Calvin cycle, chloroplast H^+-ATPase as well (Schwarz *et al.*, 1997). Trx m does not show the same features, instead, it resembles *E. coli* thioredoxin (*E. coli* Trx) both in activity and structure, sharing 46 % sequence iden-

tity with it (Jacquot *et al.*, 1997). Trx m and *E. coli* Trx have been reported to be unable to activate FBPase (Tsugita *et al.*, 1983), or, under *in vitro* conditions quite different from *in vivo* conditions, at most perform this task marginally (Geck *et al.*, 1996; Häberlein & Vogeler, 1995). The main role of Trx m in the chloroplast was thought to be the activation of the NADP-dependent enzyme malate dehydrogenase. However, this enzyme is also very efficiently activated by Trx f (Geck *et al.*, 1996; Hodges *et al.*, 1994). Recent reports indicate that thioredoxin *m* is involved in the regulation of glucose 6-phosphate dehydrogenase (Wenderoth *et al.*, 1997) and probably in other metabolic processes in chloroplasts (Danon & Mayfield, 1994; Jacquot *et al.*, 1997; Levings & Siedow, 1995). Both Trx f and Trx m regulate the activity of chloroplast enzymes by thiol disulfide interchange mechanisms and, in order to do so, they need to be reduced by ferredoxin:thioredoxin reductase in the presence of photoreduced ferredoxin (Jacquot *et al.*, 1997). This regulatory system is, therefore, light-activated.

Extensive structural data are available for several thioredoxins. The three-dimensional structures, determined by X-ray diffraction, have been reported for oxidized thioredoxin from *E. coli* (Holmgren *et al.*, 1975; Katti *et al.*, 1990), for a thioredoxin from the cyanobacterium *Anabaena* (Saarinen *et al.*, 1995) and for oxidized and reduced human Trx (Weichsel *et al.*, 1996). Solution structures of oxidized and reduced thioredoxin from *E. coli* (Jeng & Dyson, 1994), of reduced human Trx (Forman-Kay *et al.*, 1991), of a thermostable thioredoxin from *Bacillus acidocaldarius* (Nicastro *et al.*, 2000) and of a cytoplasmic (Mittard *et al.*, 1997) and of a *m*-like thioredoxin from *Chlamydomonas reinhardii* (PDB entry 1DBY, unpublished results) are also known. In addition, X-ray and NMR structures of mutant thioredoxins and thioredoxin-target peptide complexes have been reported (Andersen *et al.*, 1997; De Lorimier *et al.*, 1996; Nikkola *et al.*, 1993; Qin *et al.*, 1995, 1996). The aim of the studies reported here is a structural comparison of spinach chloroplast Trx f and Trx m at the three-dimensional level, to provide a structural basis for their functional differences. Two further issues are addressed in this analysis: the conformational behavior of the Trx m active-site disulfide upon reduction and a test of existing hypotheses about a distinct evolutionary origin for Trx f and Trx m.

Results and Discussion

Structure determination of thioredoxin f (short and long forms)

The elucidation of the three-dimensional structure of Trx f has been a long-standing goal in the thioredoxin field. The high distinction between the Trx f amino acid sequence and those of the rest of the family, and its very high specificity in target enzyme activation, suggested structural peculiarities which might be disclosed by X-ray crystallography. The present report describes the structure of Trx f both in a "long" (Trx f-L) and in a "short" (Trx f-S) form, which crystallize in the same space group, but with different cell dimensions and packing. The Trx f-L construct, used in the early studies (Aguilar *et al.*, 1992; Génovésio-Taverne *et al.*, 1991) proved rather insoluble and difficult to crystallize. Therefore, the final effort was concentrated on Trx f-S, at the N terminus truncated Trx f, which is more soluble (DelVal *et al.*, 1999). Efficient crystallization conditions for the latter were found easily (see Materials and Methods), and many crystals could be grown, allowing molecular replacement and isomorphous replacement attempts to be carried out in parallel. Isomorphous replacement attempts quite soon provided good phases (Table 1). An uranyl nitrate derivative, in particular, yielded a strong anomalous signal which allowed the calculation of a very clean anomalous difference Patterson map that was instrumental in finding the coordinates of the two main uranyl sites. The SIRAS phases calculated from these two sites, further improved through density modification, were already good enough to produce an interpretable electron density map. Molecular replacement worked well when, at a later stage, the human thioredoxin crystal structure became available (Weichsel *et al.*, 1996). Crystallographic data for Trx f-S were of high quality and very complete (Table 1), resulting in good geometry and good crystallographic statistics for the final refined atomic model. Furthermore, the presence of two molecules in the asymmetric unit enabled effective phase improvement through twofold averaging. The final refined Trx f-S model was used to obtain a straightforward molecular replacement solution for the Trx f-L crystal form (Génovésio-Taverne *et al.*, 1991) of which an earlier data set at 1.85 Å resolution, but of lower quality and completeness, collected on a FAST area detector system, was available (Table 1). Rigid-body refinement of the molecular replacement solution, carried out between 8.0 and 1.8 Å, resulted in an *R*-factor of 43.4 % and a correlation coefficient of 74.9 %. Structure refinement involved substantial manual building intervention, not only due to the presence of 13 additional residues, but also to significant structural differences and to a generally slightly lower quality of the density. The difference in map quality is most likely caused by the inherently poorer data collection method and by the less advanced processing routine used for FAST data as compared to the imaging plate data available for the Trx f-S. After careful refinement, a Trx f-L structure of very good stereochemistry could nonetheless be obtained. At the end of the refinement, the Trx f-L structure displayed continuous and good quality density for residues 1-121, and the Trx f-S structure continuous and high quality density for residues 10-121 (Figure 2). The *R*-factor and *R*-free factor were 20.9 % and

Table 1. Trx f data collection and phasing statistics

	Trx f-S Native	Trx f-L Native	Trx f-S *cis*-platinum	Trx f-S $HAu(NO_3)_4$	Trx f-S $UO_2(NO_3)_2$
Data collection facility	Imaging plate	FAST area detector	Imaging plate	Imaging plate	Imaging plate
Heavy-atom concentration (mM)			5	2	3
Soaking time			8d	33d	3h
No. of sites			2	2	2
Unique reflections	20,015	9180	7373	6066	5829
Multiplicity	2.9	[a]	3.6	2.9	3.2
Completeness (%)	98.9	95.2	98.7	99.6	97.9
Highest resolution (Å)	1.86	1.85	2.6	2.8	2.8
R_{sym} (%)[b]	8.2	3.5	5.8	8.3	5.0
R_{iso} (%)[c]			16.4	17.4	31.2
R_{ano} (%)[d]			8.2	11.3	11.0
R_{Cullis} (%)[e]			0.505	0.579	0.548
R_{Kraut} (%)[f]			0.112	0.130	0.192
Phasing power[g]			1.82	1.45	1.92

[a] Due to unfortunate circumstances, this value could not be recovered from the records of Génovésio-Taverne *et al.* (1991).

[b] $R_{sym} = \Sigma_{hkl}\Sigma_j|I_{j,hkl} - \langle I_{hkl}\rangle|/\Sigma_{hkl}\Sigma_j I_{j,hkl}$ where $\langle I_{hkl}\rangle$ is the average of the intensity $I_{j,hkl}$ over $j = 1, \ldots, N$ observations of symmetry equivalent reflections *hkl*.

[c] $R_{iso} = \Sigma_{hkl}||F_{ph}| - |F_p||/\Sigma_{hkl}|F_p|$, where F_p and F_{ph} are the structure factor amplitudes of the native protein and heavy-atom substituted protein, respectively.

[d] $R_{ano} = \Sigma|\langle I^+\rangle - \langle I^-\rangle|/\Sigma|\langle I^+\rangle + \langle I^-\rangle|$, i.e. measure of the mean relative anomalous difference between the Bijvoet pairs.

[e] $R_{Cullis} = \Sigma_{hkl}||F_{ph} \pm F_p| - F_h(calc)|/\Sigma_{hkl}|F_{ph} - F_p|$, where F_{ph}, F_p and $F_h(calc)$ are the derivative and native amplitudes and the calculated heavy-atom structure factors, respectively.

[f] $R_{Kraut} = \Sigma_{hkl}||F_{ph}| - F_{ph}(calc)|/\Sigma_{hkl}|F_{ph}|$, where F_{ph} and $F_{ph}(calc)$ are the derivative amplitudes and calculated derivative structure factors, respectively.

[g] Phasing power $= \Sigma_{hkl}F_h/\Sigma_{hkl}||F_{ph}| - F_{ph}(calc)|$, where F_{ph} and $F_{ph}(calc)$ are the derivative amplitudes and calculated derivative structure factors, respectively, and F_h is the calculated heavy-atom structure factor.

26.8 %, respectively, for Trx f-L and 19.7 % and 23.7 %, respectively, for Trx f-S (for details, see Table 2). The higher difference between the two indicators, which is observed in Trx f-L, can be attributed not only to lower data quality, but also to the presence of only one molecule per asymmetric unit as opposed to two molecules in the case of Trx f-S. The rmsd value between the equivalent atoms of the superimposed NCS-related Trx f-S molecules (C^α atoms only) is 0.2 Å. The stereochemical quality of both Trx f structures is very good and there are no outliers in the Ramachandran plots of either of them.

Overall structure description of thioredoxin f and differences between its long and short form

Trx f retains the overall thioredoxin fold (Katti *et al.*, 1990), consisting of a five-stranded mixed β-sheet, flanked by four helices arranged in the common thioredoxin secondary structure motif β1, α1, β2, α2, β3, α3, β4, β5, α4 (Figure 3). In addition, Trx f-L contains another short helix at the N terminus encompassing, according to PROMOTIF (Hutchinson & Thornton, 1996), residues 6 to 12, while residues 1 to 5 adopt a rather extended conformation (Figure 4(a)). The additional N-terminal helix is up to now unique among thioredoxin structures and it seems appropriate to call it α0. An analysis of the Trx f-L structure reveals that helix α0 forms a single, compact unit with the rest of the protein and lies far away from the active site, on the opposite side of the molecule. It is interesting that in the short form (Trx f-S), which begins with residue 10, the region between Met10 and Ile13 adopts a coil conformation (Figure 4(a)). This important difference might be caused by the absence of residues preceding Met10, but crystal packing might also play a role.

Another important difference between the two forms concerns the conformation of the active site peptide, which appears to be influenced by the crystal packing. Whereas Trx f-L crystallizes with only one molecule in the asymmetric unit, in Trx f-S two molecules, related by a non-crystallo-

Table 2. Trx f refinement statistics

Data set	Trx f-S	Trx f-L
Resolution range (Å)	25.5-1.86	25.6-1.85
R_{cryst} (%)[a]	19.7	20.9
R_{free} (%)	23.7 (4.8 % of the data)	26.8 (3.1 % of the data)
Number of atoms	1894	977
Protein	1752 (2 molecules)	943 (1 molecule)
Solvent	142	34
rmsd bond lengths (Å)	0.01	0.01
rmsd bond angles (°)	1.3	1.3
Ramachandran plot regions (%)		
Most favorable	89.4	91.6
Additionally allowed	10.6	8.4
Overall *B*-factor	22.3	34.2
Wilson *B*-factor	19.8	25.6

[a] $R_{cryst} = (\Sigma_{hkl}||F_o| - |F_c||)/\Sigma_{hkl}|F_o|$, where $|F_o|$ and $|F_c|$ are the observed and scaled calculated structure factor amplitudes, respectively.

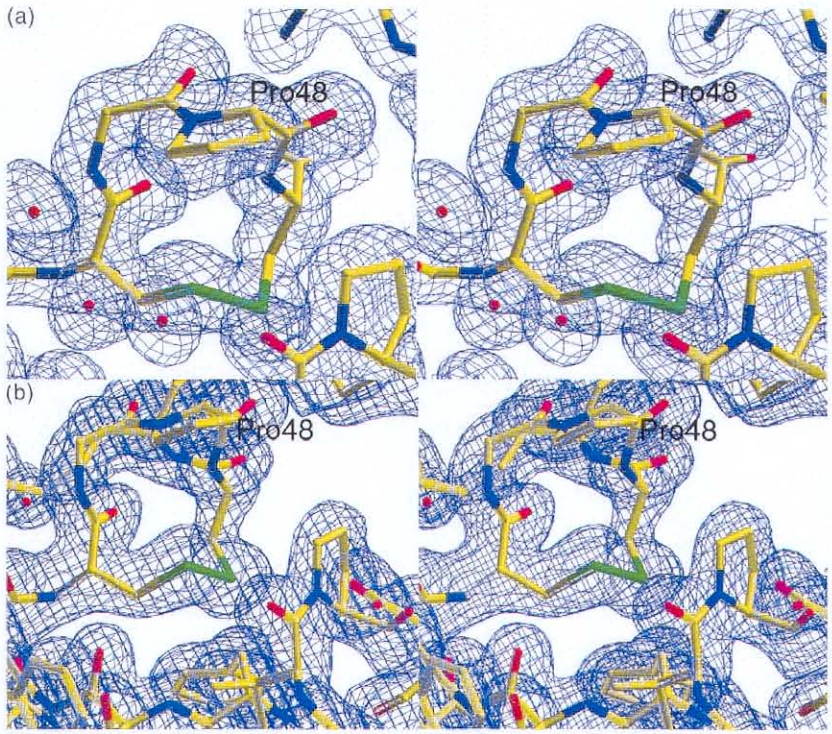

Figure 2. Active site views of Trx f-S and Trx f-L. (a) Stereo view of the Trx f-S active site. Residues are depicted in yellow and atom colors (green for the sulfur of the disulfide bridge), water molecules appear as red spheres. Pro48, part of the WCGPC active-site motif, is labelled in black. The final $2F_o - F_c$ map, contoured at 1.0σ, is superimposed on the atomic model. (b) The Trx f-L active site in a similar view. Details as above. Prepared with the program O (Jones & Kjeldgaard, 1991).

graphic 2-fold axis, pack quite tightly together with the active site regions facing each other. In Trx f-S the indole group of Trp45 of one molecule stacks onto the side-chain of Ile86 from its NCS-related partner. In order to achieve such a good stacking, the Trp side-chain had to "flip out" (Figure 4(b)) with respect to its usual position, as found in Trx f-L, and, for instance, in *E. coli* thioredoxin (Katti *et al.*, 1990). In addition, the side-chain of Gln44 of Trx f-S has flipped over to the opposite side also. Apart from these differences, the Trx f-L and Trx f-S structures are essentially identical with the rmsd value between the 110 common C^{α} atoms being 0.5 Å.

As already mentioned, in the Trx f-L structure residues 1 to 5 take up a rather extended conformation, entering helix α0 from an angle of about 120° to its axis. It is notable that this extended stretch makes an intimate contact with the active site of a Trx f molecule from a neighboring unit cell (Figure 4(c)). In the crystal structure of thioredoxin 2 from *Anabaena* (*Anabaena* Trx; Saarinen *et al.*, 1995), an N-terminal sequence making a very similar active site contact to that of Trx f-L has been encountered. Moreover, the NMR structure of a covalent complex between human thioredoxin and a target peptide from the NFκB transcription factor (Qin *et al.*, 1995) displays an analogous situation as well: although it is covalently bound to the active site Cys32, the target peptide of human thioredoxin covers the N termini of Trx f-L and of *Anabaena* Trx rather well, when the corresponding molecules are optimally superimposed.

Thioredoxin m: packing and overall structure description

The native oxidized Trx m structure was determined at 2.1 Å resolution by straightforward molecular replacement using *E. coli* thioredoxin (*E. coli* Trx) as a search model. The final $2F_o - F_c$ map is of excellent quality, thanks to the high redundancy (8.5) and completeness (99.3 %) of the data set. The map shows well-defined and continuous density for residues 9 to 112. Data collection and refinement statistics are given in Tables 3 and 4. The asymmetric unit contains two Trx m molecules (V_M value of 2.4), which are related by a non-crystallographic 2-fold axis. The Trx m structure closely resembles that of *E. coli* thioredoxin and is locally quite different from Trx f, especially in the N-terminal region. Using DALI (Holm & Sander, 1993) as a comparison tool, the root-mean-square deviation (rmsd) between Trx m and *E. coli* Trx for 104 common C^{α} atoms is 1.0 Å, whereas the rmsd value between Trx m and Trx f-L or Trx f-S for the

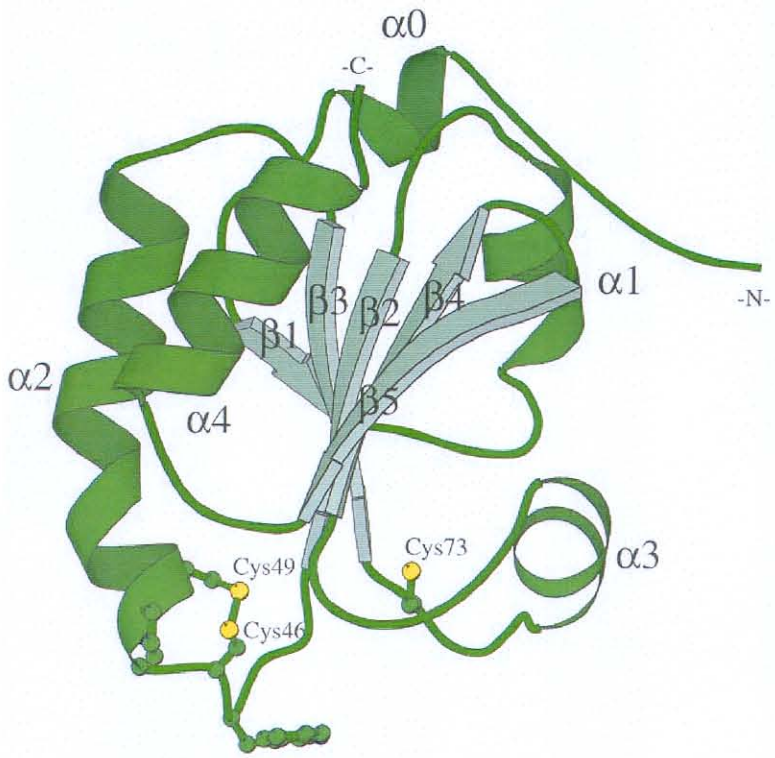

Figure 3. Cartoon representation of the Trx f-L spatial structure. Secondary structural elements are labelled according to the thioredoxin convention. The side-chains of residues of the WGGPC active site motif appear in ball-and-stick mode, as well as the side-chain of Cys73. The positions of the N terminus, C terminus and of the three cysteine residues (C46, C49 and C73) are labelled. Prepared with MOLSCRIPT (Kraulis, 1991).

common 102 C^{α} atoms is 1.2 Å. Figure 5 shows the overall structure of Trx m, while Figure 6 displays a superposition of the Trx f-L, Trx m and *E. coli* Trx C^{α} traces and active sites. In the present Trx m crystal structure, the first eight residues at the N terminus are not visible. This represents the most important large-scale structural difference between Trx f and Trx m. Whereas Trx f possesses a highly structured N-terminal region, which encompasses an additional helix and an extended stretch, the N terminus of Trx m is simply disordered, at least in the present crystal form. The first well-defined residue is Val9 in both NCS-related Trx m molecules, the C^{α} rmsd value upon superposition being 0.5 Å. In the case of Trx m, refinement was performed with strict NCS constraints in the first low-resolution stages (2.8 Å), then with NCS-restraints, which were released only in the final refinement cycle. A PROMOTIF analysis reveals that *E. coli* thioredoxin and Trx m have nearly identical secondary structural elements, whereas some slight differences emerge with respect to Trx f. Also, due to lattice effects, marginal differences in the secondary structure assignments are found between the two NCS-related Trx m molecules (details in Figure 1). From the superposition of the Trx f, Trx m and *E. coli* Trx C^{α} traces and active sites it is clear that *E. coli* Trx and Trx m superimpose very well. Trx f also displays a similar structure. The pattern of insertions and deletions is summarized

Table 3. Trx m data collection statistics

Data set	Trx m ox	Trx m red	Trx m red final
Oscillation range (°)	143	33	66
Unique reflections	14,256	10,890	10,911
Multiplicity	8.5	1.9	2.7
Completeness (%)			
Overall	99.3	94.3	94.2
Outermost data shell	92.0	91.7	81.9
Resolution limits (Å)	29.6-2.1	26.4-2.26	29.6-2.26
R_{sym} (%)[a]	8.6	7.0	11.0

[a] $R_{sym} = \Sigma_{hkl}\Sigma_j|I_{j,hkl} - \langle I_{hkl}\rangle|/\Sigma_{hkl}\Sigma_j I_{j,hkl}$ where $\langle I_{hkl}\rangle$ is the average of the intensity $I_{j,hkl}$ over $j = 1, \ldots, N$ observations of symmetry equivalent reflections *hkl*.

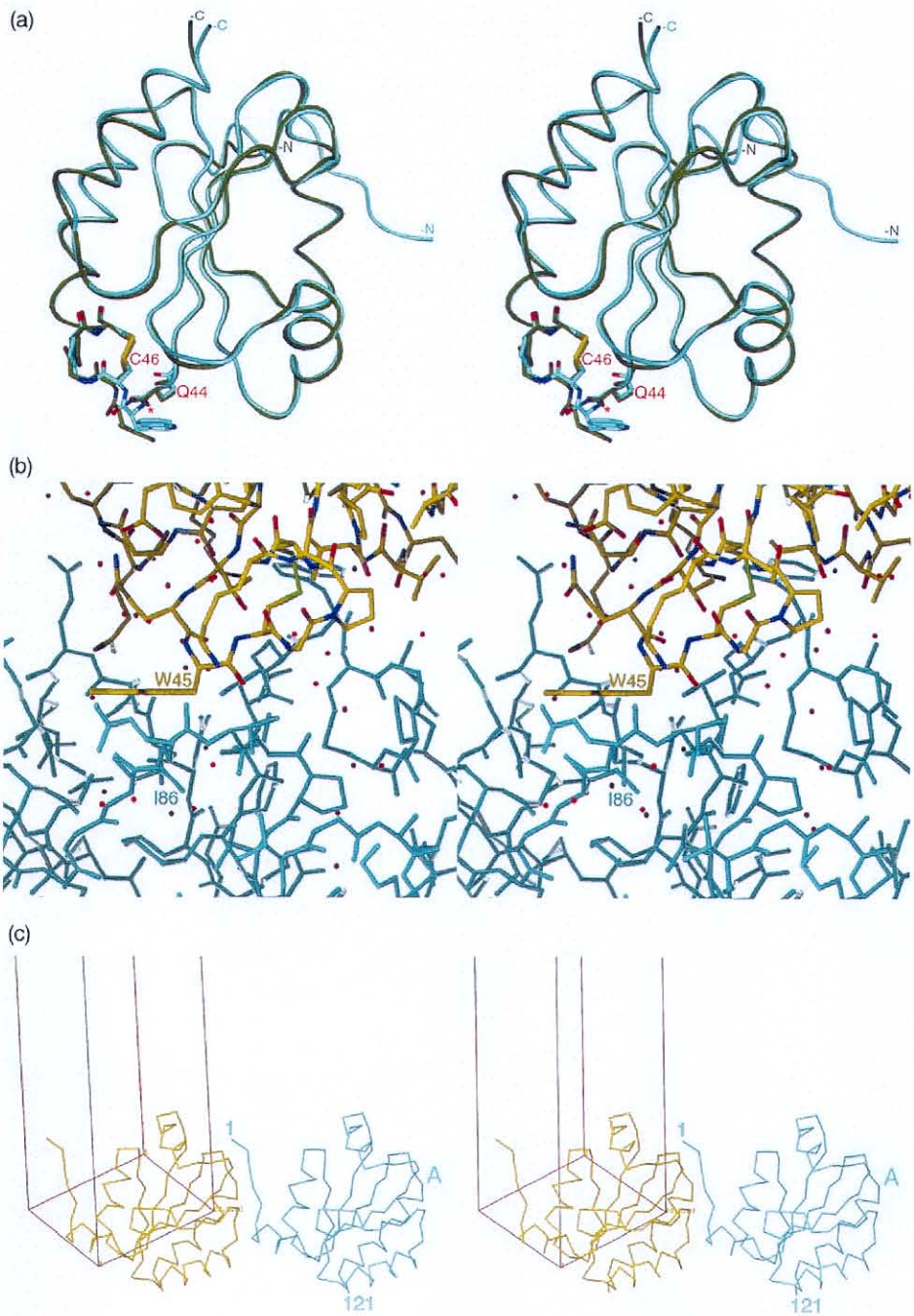

Figure 4. Particular features of the Trx f-L and Trx f-S structures. (a) Superposition of the Trx f-L (cyan) and Trx f-S (green) structures in the so-called backbone worm representation. Active-site residues from Gln44 to Cys49 appear in ball-and-stick mode, in atom colors and cyan for Trx f-L, in atom colors and green for Trx f-S. The N and C termini of Trx f-L and Trx f-S are labelled. The opposite orientations of the Gln44 to Trp45 peptide in Trx f-L and Trx f-S are emphasized by a red asterisk. Prepared with DINO (Philippsen, 1998). (b) Stereo view of the dimer interface for Trx f-S in ball-and-stick mode. Monomer A appears in atom color code and yellow, monomer B in cyan. The stacked residues Trp45 and Ile86 of the other molecule are labelled. Prepared with O (Jones & Kjeldgaard, 1991). (c) Stereo C^{α} trace representation of a Trx f-L molecule (yellow), in contact with a neighbor (cyan) from an adjacent unit cell. The active-site position is indicated by a cyan A. Prepared with O (Jones & Kjeldgaard, 1991).

Table 4. Trx m refinement statistics

Data set	Trx m ox	Trx m red initial	Trx m red final
Resolution range (Å)	29.6-2.1	26.4-2.26	29.6-2.26
R_{cryst} (%)[a]	20.4	19.8	20.5
R_{free} (%)	23.0 (3.8 % of the data)	23.5 (5.4 % of the data)	23.1 (5.5 % of the data)
Number of atoms	1765	1766	1766
Protein	1644	1653	1653
Solvent	121	113	113
rmsd bond length (Å)	0.006	0.006	0.007
rmsd bond angles (°)	1.2	1.1	1.2
Ramachandran plot regions (%)			
Most favorable	92.8	91.2	91.2
Additionally allowed	7.2	8.3	8.3
Generously allowed	0	0.6	0.6
Overall *B*-factor (Å^2)	21.3	22.2	26.9
Wilson *B*-factor (Å^2)	24.0	28.6	32.7

[a] $R_{cryst} = (\Sigma_{hkl}||F_o| - |F_c||)/\Sigma_{hkl}|F_o|$, where $|F_o|$ and $|F_c|$ are the observed and scaled calculated structure factor amplitudes, respectively.

in Figure 1, which is based on a structural alignment of Trx f-L, Trx m, *E. coli* Trx and human thioredoxin.

The active site region in Trx f and Trx m

Thioredoxins are very efficient reducing agents. They owe their thiol:disulfide oxidoreductase activity to the active site -Trp-Cys-Gly-Pro-Cys- and to the peculiar properties of the two cysteine residues. The efficiency is certainly due in part to the lowered pK_a value of the first exposed cysteine (Cys32 in *E. coli* Trx, Cys46 in Trx f and Cys37 in Trx m), which has a microscopic pK_a value close to the physiological pH (Chivers *et al.*, 1997). The mechanism by which this is achieved is still a matter of controversy (Holmgren, 1995). Several factors or specific residues in the vicinity of the active site have been made responsible (Chivers & Raines, 1997; Hol, 1985; Kortemme *et al.*, 1996; LeMaster *et al.*, 1997; Vohnik *et al.*, 1998). A second important feature is the solvent accessibility of this same cysteine. The other cysteine (Cys35 in *E. coli* Trx, Cys49 in Trx f and Cys40 in Trx m), which is not solvent accessible in *E. coli* Trx, has a pK_a value which is at least four units higher than the physiological one and therefore is relatively unreactive (Chivers *et al.*, 1997; LeMaster, 1996).

With −0.290 V (Trx f) and −0.300 V (Trx m) (Hirasawa *et al.*, 1999), both Trx f and Trx m have midpoint reduction potentials similar to those observed for other thioredoxins (Salamon *et al.*, 1992). An inspection of the active site region of the chloroplast thioredoxins shows that their geometry is essentially comparable to that of *E. coli* Trx and could allow the same reaction mechanism proposed for *E. coli* Trx (Chivers & Raines, 1997). According to this proposal, the buried, highly conserved Asp26 (Asp40 in Trx f) serves as proton acceptor in the deprotonation of Cys35 (Cys49 in Trx f) and loses a proton to solvent water. In the crystal structures of *E. coli* Trx, Trx f and Trx m this aspartate faces a cavity containing bound water molecules, compatible with the mechanism described above.

One important aspect of the thioredoxin mechanism is a slight conformational change that occurs upon reduction of the protein. This phenomenon has been described crystallographically for human thioredoxin (Weichsel *et al.*, 1996) and has also been addressed in the present studies. Attempts to reduce Trx f-S by soaking crystals in DTT-containing solutions invariably failed. Such experiments resulted in crystal disruption, crystal cracking or collection of inferior data corresponding to still oxidized Trx f. This is most probably due to the crystal packing, in which the active disulfide bridge participates in the non-crystallographic dimer interface and cannot be reduced without destroying the crystal order. On the contrary, reduction attempts were fully successful in the case of Trx m as will be described later.

So far, much fewer biochemical data for Trx f and Trx m are available than for *E. coli* Trx, and the pK_a values of Trx f Cys46 and 49 are not known. However, the structural similarities between the Trx f and *E. coli* Trx active sites speak in favor of the same reaction mechanism for the two proteins. The question then remains, why only Trx f can effectively activate FBPase, whereas *E. coli* Trx (or also Trx m) can not. The answer probably resides in the surface properties of the different thioredoxins (Figure 7). It is well known that non-covalent complexes can be formed between thioredoxins and their target enzymes, and complex formation has been invoked in order to explain kinetic data (Braun *et al.*, 1996; Häberlein & Vogeler, 1995). In the case of spinach Trx f and FBPase a K_d value of 800 nM was reported for the non-covalent complex (Soulié *et al.*, 1985), strong enough for employing complex formation as a purification tool (Pla & Lopez-Gorge, 1981). No stable complex of spinach Trx m with FBPase has been observed, although kinetic evidence for it has been reported (Häberlein & Vogeler, 1995). In an attempt to find an expla-

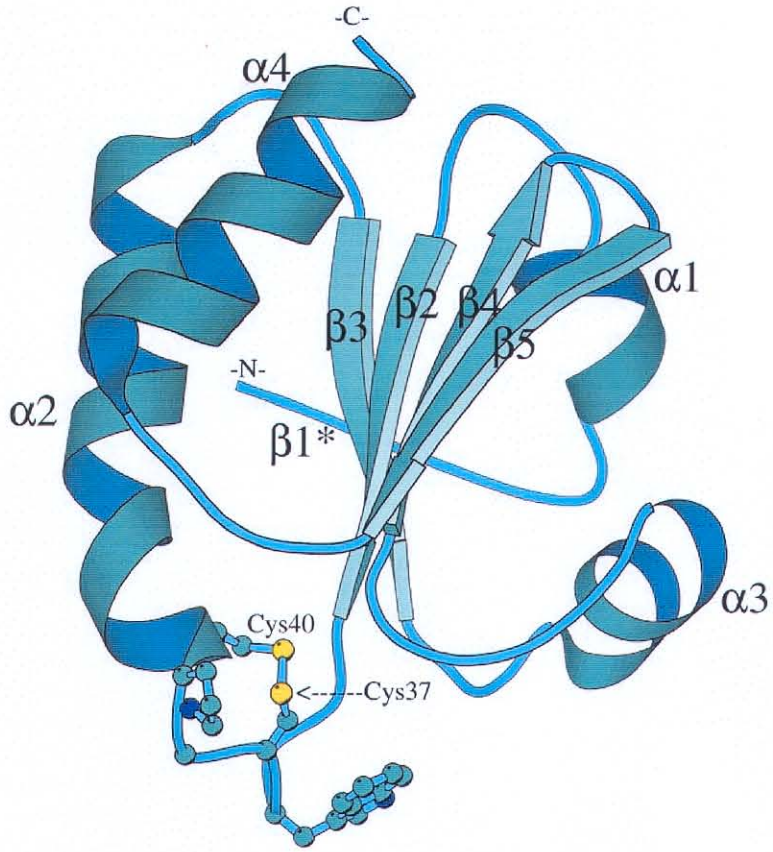

Figure 5. Cartoon representation of the Trx m structure (molecule B). The asterisk empasizes a β-strand (β1) of two residues, too short for being drawn as an arrow by the program. Secondary structural elements are labelled according to the thioredoxin convention. Residues of the WCGCP active site motif appear in ball-and-stick mode. The N and C termini and the active site cysteine residues 37 and 40 are labelled. Prepared with MOLSCRIPT.

nation for these functional differences, a comparative analysis of surface properties for Trx f and Trx m was carried out.

The third cysteine of thioredoxin f

Among the sequence peculiarities of Trx f is the presence of a third, surface-accessible conserved cysteine (Cys73). This third cysteine residue is responsible for the appearance of a thioredoxin f dimer upon electrophoretic separation, a behaviour neither observed for spinach Trx m, which has no additional cysteine residues, nor with mutants of Trx f lacking this cysteine (C73A, C73S or C73G) (DelVal *et al.*, 1999). In human thioredoxin, which possesses even three further exposed cysteine residues, dimer formation *via* an intermolecular disulfide bond has been demonstrated by protein crystallography. The effect was interpreted as a possible regulatory mechanism (Andersen *et al.*, 1997), a hypothesis which, however, has recently been challenged by NMR-based studies (Gronenborn *et al.*, 1999).

In both Trx f-L and Trx f-S, Cys73 is clearly reduced and does not form any significant intermolecular contact. The dimer interface of Trx f-S, calculated by following the recommendations of Janin (1997), is of non-covalent nature and buries a surface of 578 Å^2. As already mentioned, Trx f-L crystallizes with one molecule per asymmetric unit and its crystal contacts differ markedly from those of Trx f-S.

The mutational studies by DelVal *et al.* (1999) have pinpointed Cys73 as the residue responsible for the dimer formation observed *in vitro*, and as a critical residue for the Trx f-FBPase interaction, by demonstrating that the C73G, C73A and C73S mutants are much less efficient than wild-type Trx f in activating the target enzyme. The impairment is most dramatic in the Cys to Gly mutant. In the other two cases the effect is less severe, with the Cys to Ala mutant being slightly less efficient than the Cys to Ser mutant.

The specificity of Trx f: role of surface properties

As mentioned above, in order to understand the functional differences between Trx f and Trx m it is important to compare their surface properties. Considering the fact that the overall structures of the two proteins are very similar, differences in activity and specificity likely reside in the residues forming the docking area for target enzymes around the active site. According to a widely accepted view of protein-protein interactions,

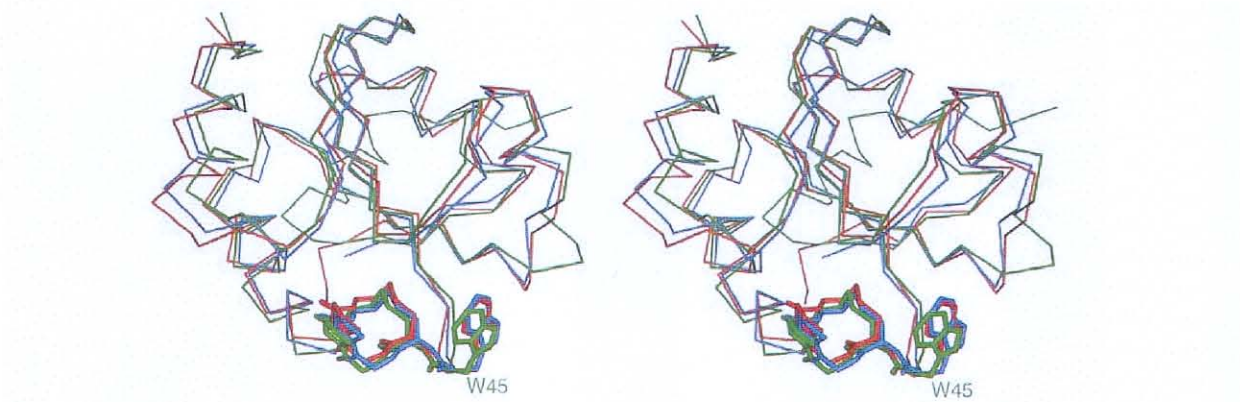

Figure 6. Superimposed stereo C^{α} traces of the Trx f-L (green), Trx m (blue) and *E. coli* Trx (red) structures. The active-site residues appear in ball-and-stick mode. The active-site tryptophan 45 of Trx f-L is labelled. Prepared with DINO (Philippsen, 1998).

complementary charge distributions on the surfaces of thioredoxin and of its target enzyme define the relative orientation of the partners when they approach each other. When the two proteins approach each other more closely, hydrophobic effects, correlated with surface complementarity, start playing an important role. The crystal structure of a prime Trx f target enzyme, spinach FPBase, has been known for some time (Villeret *et al.*, 1995). This allows, in principle, docking attempts with Trx f that might reveal the determinants for the specific complex formation. The docking site for thioredoxin on FBPase, as identified biochemically (Sahrawy *et al.*, 1997), corresponds to a flexible loop of 16 amino acid residues, representing an insertion in the sequence not present in animal FBPases (Marcus *et al.*, 1988). In the spinach FBPase crystal structure, in which the whole homotetramer forms the asymmetric unit, this loop assumes a different conformation in each of the four subunits, ruling out the possibility of straightforward docking. Recently, the crystal structure of pea FBPase in the oxidized form was determined (Chiadmi *et al.*, 1999). It revealed the location of the regulatory disulfide bridge in the pea enzyme and provided a starting template for homology modelling of spinach oxidized FBPase and docking attempts with spinach Trx f. These issues will be addressed in future research work. Comparison of the reduced spinach and of the oxidized pea FBPases suggested that, upon reduction of the disulfide bridge by thioredoxin, the secondary structure of the regulatory region melts and triggers a movement of the β1-β2 strands, resulting in a catalytically competent conformation of the active site (Chiadmi *et al.*, 1999). The regulatory region of spinach FBPase contains three cysteine residues (Cys155, Cys174 and Cys179), two of which are believed to form the regulatory disulfide bridge that undergoes attack by Trx f Cys46 (Brandes *et al.*, 1993). By analogy with the structure of oxidized pea FBPase, the regulatory cysteine residues in the spinach enzyme should be Cys155 and Cys174, with the latter being exposed to the solvent and the former being completely buried. We focus here on the analysis of the Trx f and Trx m surface properties. Figure 7 displays the surfaces of Trx f (Figure 7(a)) and Trx m (Figure 7(b)) colored according to residue type. Upon comparing the two surfaces, the green spot corresponding to Trx f Cys73, which site-directed mutagenesis has identified as important for FBPase activation (DelVal *et al.*, 1999), is immediately apparent in the depression to the left of the active site. The corresponding region in Trx m is of a polar nature. If one compares the area which surrounds the active site cysteine residues in Trx f with the corresponding region of Trx m, the distribution of hydrophobic patches and charged amino acid residues is seen to differ substantially (Figure 7(a) and (b)). The distribution of the electrostatic potential on the Trx f and Trx m surfaces also exhibits differences, with Trx f being in general more positively charged (Figure 7(c)) and Trx m displaying a compact, strongly negatively charged patch near the active site Trp36 (Figure 7(d), see below for the differences between the active site Trp of Trx f-L, Trx f-S and Trx m). Figure 8 summarizes the comparison of Trx f and Trx m through a conservation/divergence approach based on a structural alignment. The conserved residues between Trx f and Trx m appear in red on the Trx f-L surface, those that are partially conserved in yellow (Figures 1 and 8(a)). Those Trx f residues for which there is a charge difference of ±1 with their Trx m counterparts are depicted in dark cyan, those which have opposite charges are depicted in magenta (Figure 8(b)). "Cyan" and "magenta" residues are found at the periphery of the active site area and more distant areas. They are not found in the immediate vicinity of the active site, which suggests that the contact area with FBPase may be rather large. A factor which limits the efficacy of analyses based on sequence comparison is

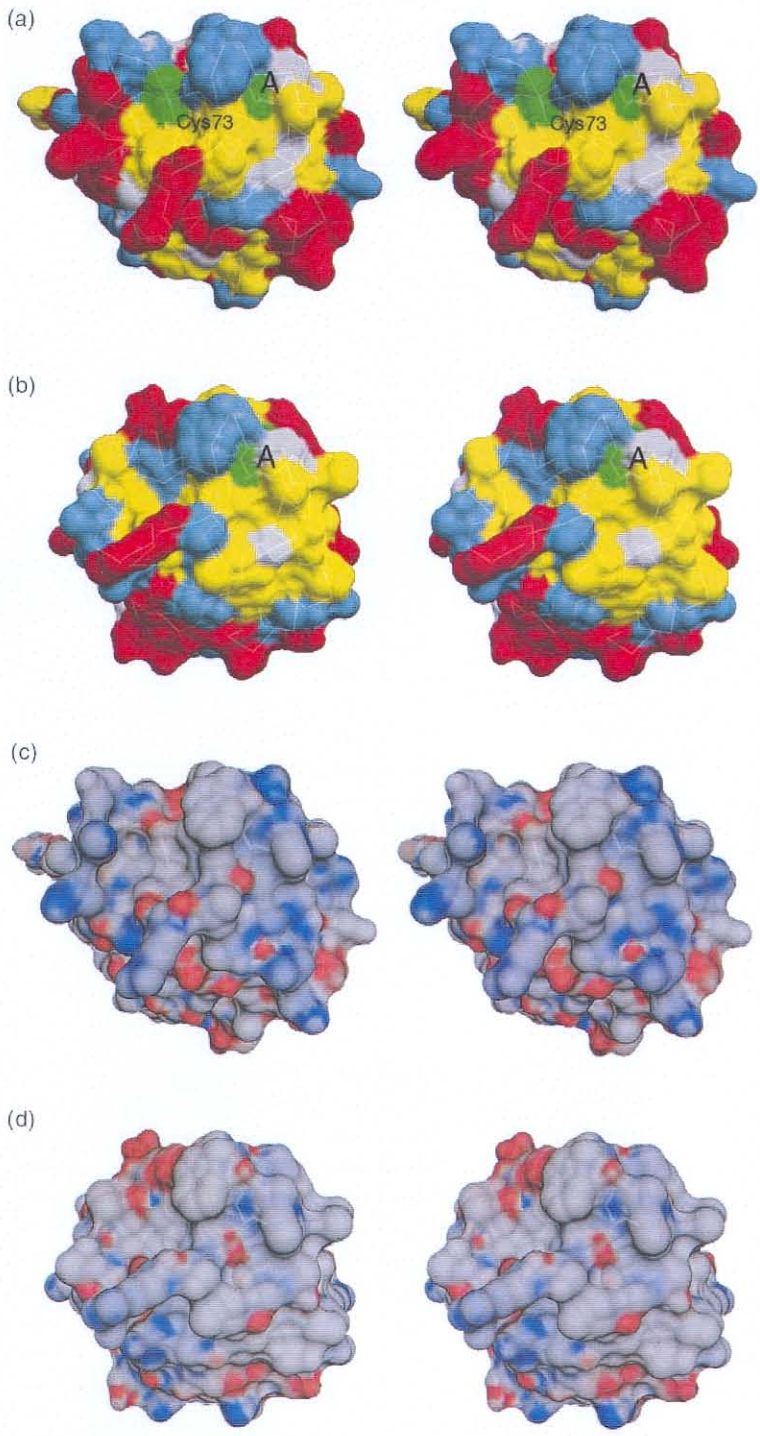

Figure 7. Stereo surface representations of Trx f-L and Trx m. (a) Trx f-L, mapped by residue type. Parts of the surface contributed by polar residues appear in blue, by charged residues in red, by hydrophobic residues in yellow and by cysteine residues in green. The side-chains of the active site cysteine residues and of Cys73 are depicted in ball-and-stick mode and they are visible, along with the C^{α} traces, behind the semi-transparent surfaces. The active site (A)′ and Cys73 are labelled in black. Trx m, mapped by residue type. Colour codes as above. The active site (A) is labelled in black. (b) Trx f-L, mapped by electrostatic surface potentials (red, negative; blue, positive) as calculated with the GRASP Poisson-Boltzmann "solver". (d) Trx m, mapped by electrostatic surface potentials, in the same way as above. Prepared with GRASP (Honig & Nicholls, 1995), MSMS (Sanner *et al.*, 1996) and DINO (Philippsen, 1998).

"evolutionary noise". One has to take into account that, most probably, only a fraction of the differences appearing in Figure 8 have a functional significance. Mora-García *et al.* (1996) have analyzed the role of electrostatic interactions on the affinity of *E. coli* Trx for target proteins. They found that the mutants E30K, L94K and E30K/L94K *E. coli* Trx, designed with the aim of approaching the putative charge distribution of Trx f, were significantly better than the wild-type ($A_{0.5} = 33$ μM) at activating FBPase (which has a negatively charged regulatory loop), with $A_{0.5}$ values of 9 μM (E30K), 7 μM (L94K) and 3 μM (E30K/L94K). The wild-type Trx f was still more efficient and exhibited an

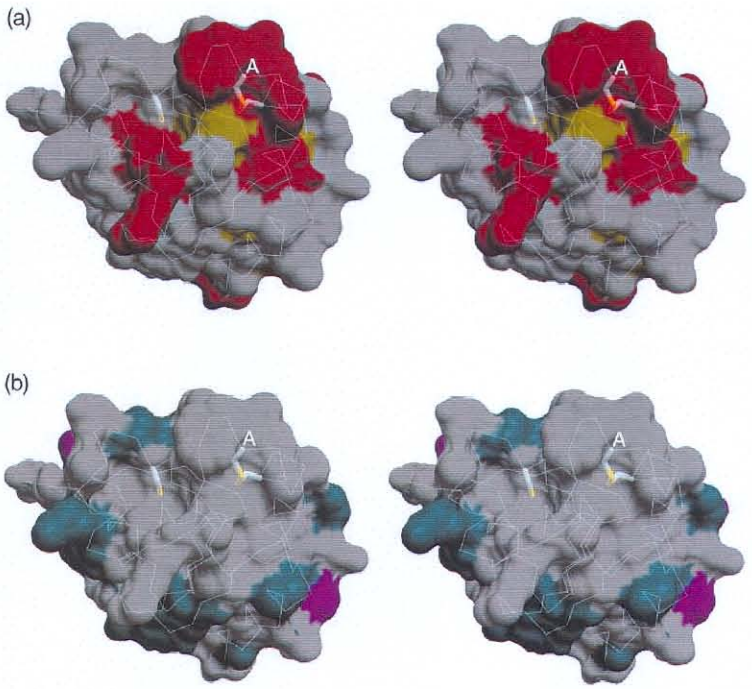

Figure 8. Stereo surface representation of Trx f as mapped according to the structural alignment with Trx m (Figure 1). The active-site position is indicated by a white A. (a) The residues conserved in both Trx f and Trx m appear in red on the Trx f surface, the partially conserved ones in yellow. (b) Those residues for which there is a charge difference of ±1 between Trx f and Trx m are depicted in dark cyan, those which have opposite charges (difference of ±2) are depicted in magenta. The side-chains of Cys46, Cys49 and Cys73 appear in (a) and (b) in ball-and-stick mode, and can be seen, along with the C^{α} traces, behind the semi-transparent surfaces. Prepared with DINO (Philippsen, 1998) and MSMS (Honig & Nicholls, 1995).

$A_{0.5}$ of 0.9 μM. Comparison with the experimental Trx f structure shows that the *E. coli* Trx L94K mutant introduces a positive charge at the spatial position corresponding to Lys108 of Trx f and to Val99 of Trx m. Lys30 in the *E. coli* Trx E30K mutant corresponds spatially to Gln44 of Trx f, a polar residue, and to Pro35 of Trx m. The importance of electrostatic contributions in the interactions of wt Trx f, wt *E. coli* Trx and of the three aforementioned Trx mutants with target enzymes was stressed by shielding experiments with high concentrations of neutral salts (Mora-García *et al.*, 1996). The $A_{0.5}$ value of wt *E. coli* Trx and of the three mutants, for example, converges towards a common value of ≈9 μM in the presence of high concentrations of KCl. The $A_{0.5}$ value for Trx f, on the contrary, does not converge, which was tentatively attributed to a contribution of other structural factors to the Trx f-FBPase docking (Mora-García *et al.*, 1996). The Trx f-S and Trx f-L atomic models presented here provide a clue to the nature of such putative structural factors.

Active site flexibility in Trx f: a structural clue to specifity?

Trx f-S and Trx f-L exhibit different conformations in their active site regions. The greatest effect is observed at residue Trp45, as is evident in a superimposition of the Trx f-S and Trx f-L active site structures (Figure 9). Such a difference can be understood if one compares the Trx f structures to those of Trx m and *E. coli* Trx. In the latter two proteins, the Trp indole makes a hydrogen bond with the carboxyl group of a neighboring aspartate. The residues involved are Trp31 and Asp61 in *E. coli* Trx, Trp36 and Asp66 in Trx m. Trp45 of Trx f, on the contrary, cannot make such a hydrogen bond, because the residue corresponding to Trx m Asp66 (or *E. coli* Trx Asp61) is an asparagine (Asn74), the side-chain of which points in the opposite direction and receives a hydrogen bond from the main-chain nitrogen of Asn77 (Figure 9). Asn74 in Trx f is followed by an insertion (Gln75) with respect to *E. coli* Trx, human Trx and Trx m (Figure 1). This modifies the loop conformation (residues 74 to 77) with respect to the other three structures, keeping the Asn74 side-chain away from Trp45. A multiple sequence alignment of 77 thioredoxin sequences from the SWISS-PROT database (Bairoch & Apweiler, 1997) identifies the presence of Asn74 (instead of Asp) and the inserted Gln75 as distinctive features of Trx f. In fact, the position corresponding to Asn74 is occupied by an aspartate residue in 70 sequences out of 77 and by an asparagine residue in only two cases, i.e. in the spinach and pea f-type thioredoxins. Of the remaining five sequences, two have Glu, two Thr and one Ser. This deviating local conformation may represent an important structural factor contributing to the specificity of Trx f, possibly allowing a docking mode to FBPase which is precluded or more difficult for other thioredoxins. It must be noted that the "usual" Trp-Asp interaction observed in *E. coli* Trx and Trx m is not strong and can be disrupted by crystal packing forces. In the X-ray structure of the K36E mutant of *E. coli* Trx (Nikkola *et al.*, 1993), Trp31 is involved in lattice

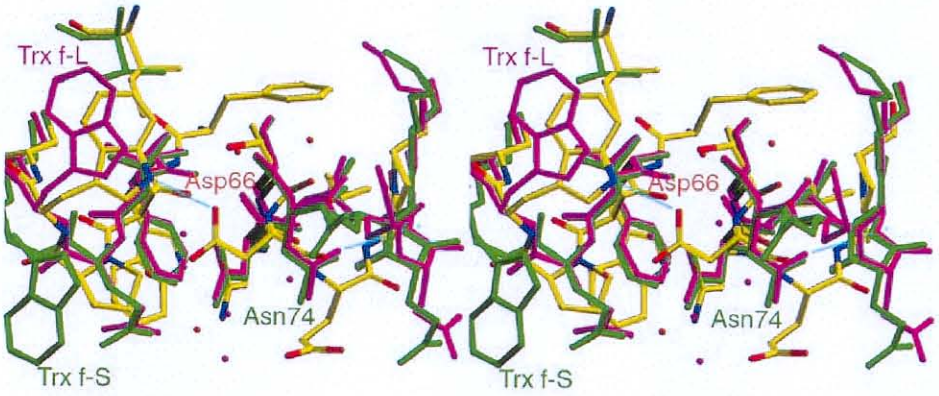

Figure 9. Stereo view of the superimposed Trx f-L, Trx f-S and Trx m ball-and-stick atomic models in the active site region centered around Asp66 (Trx m). The Trx m model is depicted in yellow and atom colors, the Trx f-S model in green and that of Trx f-L in magenta. Water molecules appear as red spheres. The residues Asp66 (Trx m) and Asn74 (Trx f) are labelled, as are Trp45 of Trx f-L (green label) and of Trx f-S (magenta label). The hydrogen bond between Asp66 and Trp36 in Trx m, as well as that between Asn74 and Asn77 in Trx f are drawn as light cyan lines. Prepared with DINO (Philippsen, 1998).

contacts: it does not interact with Asp61 and the active site conformation is similar to that observed in Trx f-S.

Some years ago, *E. coli* Trx Asp61 was mutated to Asn, with the rationale of deleting a negative surface charge (de Lamotte-Guéry *et al.*, 1991). The mutant performed better than wt *E. coli* Trx in activating FBPase, thus displaying a Trx f-like activity. This gain can be explained with electrostatic factors, as for the Trx mutants described by Mora-García *et al.* (1996). An additional structural argument may, however, play a role as well: the mutation Asp61 to Asn in *E. coli* Trx would have a weakened hydrogen bond to Trp (the charge-dipole component between the Asp charge and the indole N-H dipole would be lost), probably resulting in an increased mobility of the tryptophan itself. Trx f represents the case in which the mobility of the tryptophan would be maximum. If this interpretation is correct, a double mutant of *E. coli* Trx (D61N with insertion of a Gln after that position) should display an even higher Trx f-L activity than the D61N single mutant. This will be addressed in future biochemical and structural studies.

Reduction of thioredoxin m in the crystal

The observation that the active site disulfide bridge of Trx m (Figure 10(a)) is not involved in intermolecular contacts prompted us to attempt reduction experiments with Trx m crystals. During soaking experiments with DTT at increasing concentrations (up to 9 mM) the crystals showed clear signs of stress. Nevertheless they still retained birefringence under polarized light and it was possible to perform a very long data collection from one of these crystals (Tables 3 and 4). The crystal mosaicity value computed from the "reduced" data was higher than for the oxidized Trx m (0.38° *versus* 0.29°, respectively). In order to check whether time-dependent changes occurred in the reduced crystal, the data were split into an "initial" and a "final" dataset, each retaining an acceptable completeness of around 94%. The two datasets were separated in time by an interval of around five hours. The electron density map corresponding to the "initial" reduced Trx m data set shows at the active site an unambiguously reduced disulfide with the active Cys37 pointing outwards and the two sulfhydryl groups sharply separated (Figure 10(b)). The water molecule W117, which in the oxidized structure (Figure 10(a)) lies close to the sulfur of Cys37 and donates a hydrogen bond each to this sulfur and to the main-chain carbonyl of Ile80 is no longer visible in the reduced structure, probably because it would be too close to the new position of the sulfur atom of Cys37. In the electron density map corresponding to the final reduced Trx m dataset (Figure 10(c)), the densities of the two sulfhydryl groups are no longer discontinuous and the apparent S-S distance is reduced by 0.9 Å (molecule B) compared to the "initial" reduced Trx m structure. Our interpretation is that during the long data collection, due to oxidation, the effective DTT concentration was diminishing, and towards the end, it was no longer sufficient to keep the crystal in a fully reduced form. It is clear that the electron densities we observe correspond to time and space-averaged images. It is interesting that the phenomenon described above for molecule B is much less pronounced in molecule A. There, the apparent distance between the sulfur atoms has diminished by only 0.2 Å in the final reduced structure. Lattice and accessibility effects clearly play a role in this case. Superimposition of the active sites of oxidized and reduced Trx m reveals only small differences. A large conformational

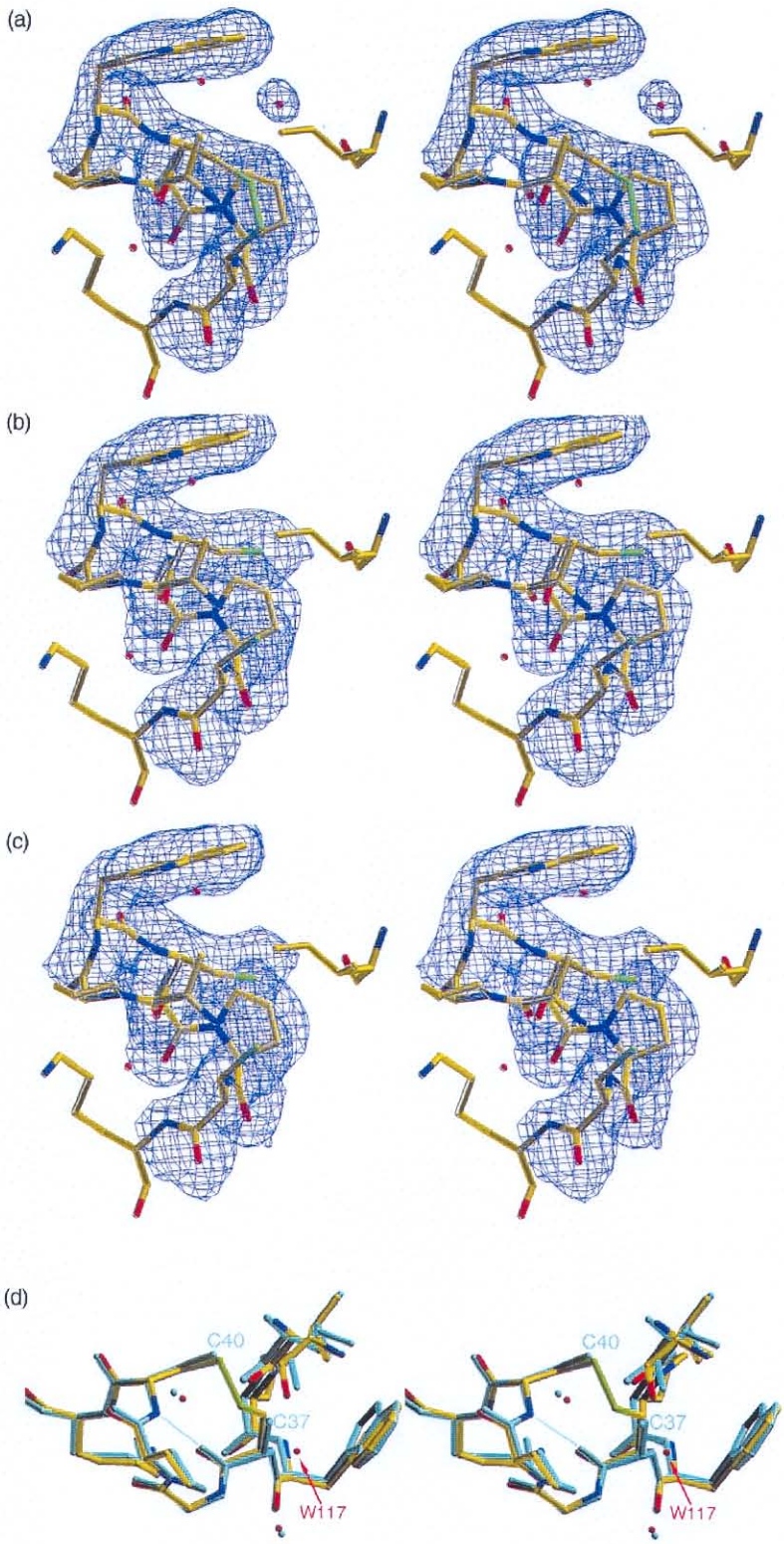

Figure 10. Stereo views of the final $2F_o - F_c$ electron density maps (contoured at 1σ) in the active-site region with the corresponding final refined Trx m models (molecule B), in yellow and atom colors, superimposed. (a) Oxidized form. (b) "Initial" reduced form. (c) "Final" reduced Trx m. (d) Superimposed active site models of the oxidized (yellow and atom colors) and initial reduced (cyan) Trx m structures. The main-chain hydrogen bond for the reduced form is depicted as a cyan lines. The active site cysteine residues, as well as water molecule W117 (not seen in the reduced structure) are labelled. Prepared with O (Jones & Kjeldgaard, 1991).

change does not occur (Figure 10(d)), which confirms the observations made for the crystal structure of human thioredoxin (Weichsel *et al.*, 1996) and for NMR work on human and *E. coli* thioredoxins (Holmgren, 1995). Upon reduction, the Cys37 sulfhydryl group "flips out", mainly through a rotation around the $\chi 1$ torsion angle, and the main-chain conformation of the -Cys-Gly-Pro-Cys- motif rearranges slightly so that a new hydrogen bond is donated by the Cys40 nitrogen to the Cys37 carbonyl. Such a "hydrogen bond switch" contributes to the stabilization of the reduced form. Due to these slight structural changes Cys37 becomes more accessible upon reduction.

One organelle, two thioredoxins. Evolutionary considerations from a structural perspective

The marked differences in sequence and activity between Trx m and Trx f have been explained from an evolutionary point of view (Tsugita *et al.*, 1983). The ubiquity of thioredoxins and thioredoxin-like proteins in living cells gives the opportunity to construct large evolutionary trees, encompassing organisms from bacteria to mammals. At present, a widely accepted theory postulates contrasting evolutionary histories for Trx f and Trx m. Classical phylogenetic analysis (Hartman *et al.*, 1990) and also comparison of intron positions (Sahrawy *et al.*, 1996) point in the same direction. Both methods indicate that Trx m is closely related to prokaryotic thioredoxins, whereas Trx f is evolutionarily distant from any other family member, although it seems weakly linked to animal thioredoxins. The consequence of this phylogenetic picture is that Trx f and Trx m, in spite of sharing the same cell compartment, cannot have a common origin. On the contrary, Trx m would have descended from the photosynthetic symbiont (a prokaryote) that gave rise to the chloroplast, whereas Trx f would have originated from an ancestor common to plants and animals.

One has to assume that during evolution the Trx m gene moved from the chloroplast to the nucleus, and adapted towards encoding a product that could be transported into the chloroplast. The same adaptation, towards encoding a transit peptide, must have been undergone by the nuclear Trx f gene (Hartman *et al.*, 1990).

Structure-based alignments are, unlike the sequence-based alignments used in phylogenetic analysis, completely reliable, with the exact pattern of insertions and deletions. Table 5 summarizes structure-based sequence comparisons of Trx f and Trx m with each other and with three other representative thioredoxin structures: human thioredoxin (PDB code 1eru), *E. coli* Trx and *Anabaena* Trx (PDB code 1thx). The comparisons were performed by superimposing the thioredoxin structures with the DALI server (Holm & Sander, 1993) and analyzing the resulting sequence identities, the rmsd values on C^{α} atoms and the DALI Z-scores. Those numbers confirm that Trx m is most similar to *E. coli* Trx (with the highest identity level and the lowest rmsd). Trx m is also significantly more similar to the other prokaryotic representative (*Anabaena* Trx), than to Trx f and human thioredoxin. Trx f shares 38 % identity and a very low rmsd value with human thioredoxin. It also exhibits a low level of identity with its chloroplastic counterpart Trx m and with the two prokaryotic thioredoxins (*E. coli* Trx and *Anabaena* Trx). The present structural results are therefore consistent with the accepted theory on evolution of chloroplastic thioredoxins, which was based on classical phylogenetic analyses.

Materials and Methods

All three thioredoxins used in these studies were recombinant proteins. They have been produced and purified according to published procedures (DelVal *et al.*, 1999; Schürmann, 1995).

Thioredoxin f

Crystallization of Trx f-S

Trx f-S was crystallized *via* the hanging drop vapor diffusion method. A 2 µl sample of protein stock solution (30 mg/ml Trx f, 50 mM Tris-HCl (pH 7.3), 0.2 M NaCl, 0.02 % (w/v) NaN_3) was mixed with an equal volume of reservoir solution containing 0.2 M $(NH_4)_2SO_4$, 0.1 M sodium acetate (pH 4.6), 25 % (w/v) PEG 4000. All experiments were performed at 20 °C. Crystals of X-ray quality appeared after several days in some of the drops

Table 5. Structure-based sequence comparison of Trx f and Trx m with each other and with three other representative thioredoxins

	Trx f			Trx m		
	Identity (%)	rmsd C^{α} atoms (Å)	Z-score	Identity (%)	rmsd C^{α} atoms (Å)	Z-score
Trx f (spinach)				31	1.2	17.2
Trx m(spinach)	31	1.2	17.2			
E. coli Trx	32	1.4	16.8	48	1.0	20.0
Human Trx	38	0.9	19.3	30	1.2	18.8
Anabaena Trx	27	1.4	15.9	34	1.0	20.1

The comparisons were performed using chain A of *E. coli* Trx and chain B of Trx m. The PDB entry codes are 2trx for *E. coli* Trx, 1eru for human Trx and 1thx for *Anabaena* Trx.

and their number could be increased by the use of the microseeding technique.

Data collection and space group determination

Data for Trx f-S were collected at 4 °C on an oscillation camera equipped with a MAR Research imaging plate detector using CuK_α radiation produced by an Elliott GX-20 rotating anode generator (40 kV, 50 mA). The space group of the crystals is $P2_1$ with cell dimensions $a = 46.59$ Å, $b = 52.56$ Å, $c = 52.57$ Å, $\beta = 108.93°$. The presence of the 2-fold screw axis was detected by inspection of systematically absent reflections. The asymmetric unit contains two Trx f molecules, related by a non-crystallographic symmetry axis. The V_M value is 2.4. The data were reduced with MOSFLM and programs of the CCP4 suite (Collaborative Computational Project Number 4, 1994): the statistics for the native data set and three heavy-atom derivatives are given in Table 1.

Structure solution

Isomorphous replacement and molecular replacement attempts were carried out in parallel. For molecular replacement the program AMORE was used. The refined coordinates of *E. coli* thioredoxin served initially as a template for the building of a search model (with the non-conserved residues trimmed to alanine). The heavy-atom derivative search happened to be faster in providing good phases than the molecular replacement method (although this also succeeded when coordinates of human thioredoxin became available and were used to build an alternative search model). Details are given in Table 1. The uranyl derivative gave rise to a high-quality anomalous difference Patterson map and to a good isomorphous difference Patterson map. From both, two sites with different y coordinate could be easily detected. This derivative allowed the calculation of good SIRAS phases, which were used to solve the other two derivatives (Table 1) by the difference Fourier method. It was then possible, by including also the anomalous signal from the Pt and the U derivatives, to calculate a MIRAS map which showed many features of the structure. The aforementioned calculations were performed with the program suite PHASES (Furey, 1989). The electron density map was further improved by density modification with DM, using solvent flattening, histogram matching and twofold averaging. The entire molecular model, except for residues 10 to 12 and 121 to 122, could then be built quickly.

The structure was also solved by molecular replacement with AMORE. A poly-alanine search model was produced based on the refined coordinates of human thioredoxin (Weichsel *et al.*, 1996). A conventional molecular replacement search (rotation, translation and rigid-body fitting for one molecule) was then performed, using an integration radius of 20 Å for the rotation search. The top-scoring solution for the single molecule search was then fixed and employed in a two-body translational search, which identified unambiguously the second molecule. The two solutions were subsequently rigid-body refined together in the resolution interval 10-3 Å (correlation coefficient 41.3 %, *R*-factor 48.7 %).

Structure refinement

The Trx f-S model was refined with X-PLOR (Brünger, 1992) against the native data, after 4.8 % of the reflections had been randomly selected to create a separate *R*-free test set. A first round of simulated annealing and positional refinement with NCS restraints on the dimer was carried out at 2.8 Å and followed by manual rebuilding. Cycles of positional and *B*-factor refinement and rebuilding were then performed at increasing resolutions of 2.5, 2.0 and 1.9 Å. In the 2.5 Å run grouped *B*-factors were used, in the subsequent ones individual *B*-factors. In the last cycle the NCS restraints were released, which resulted in slight, parallel decrease of the *R* and *R*-free factors. A bulk solvent correction was applied in order to include all low resolution data. No sigma cut-off was applied. During the refinement, difference density corresponding to residues 10 to 12 and 121 appeared, enabling completion of the model with the only exception of residue 122. Water molecules were added at positions where there was clear electron density was seen both in $F_o - F_c$ (peaks higher than 3σ) and in $2F_o - F_c$ maps, and the environment allowed reasonable hydrogen bonding to the protein or to other water molecules. The parameter file used in the refinement was PROTEIN_REP. The refinement statistics is given in Table 2. Structure validation was performed with the programs PROCHECK (Laskowski *et al.*, 1993) and WHAT_CHECK (Hooft *et al.*, 1997).

Structure solution and refinement of a "long" Trx f (Trx f-L)

The final refined model of the Trx f-S was used as a search model to solve the structure of another crystal form obtained several years ago by J.-C. Génovésio-Taverne from a longer construct carrying 12 more residues at the N terminus (Génovésio-Taverne *et al.*, 1991). This construct is three residues longer than the full-length wt Trx f sequence and contains two point mutations with respect to it. The sequences are as follows (the point-mutated residues are in bold):

```
''short''          MEAI
''wt''       MEQALGTQEMEAI
''long'' MYYLELALGTQEMEAI
```

The crystals of the long form (Trx f-L), although very difficult to obtain, diffracted well and were described by Génovésio-Taverne *et al.* (1991). They belong to space group $P2_1$, with unit cell parameters $a = 30.6$ Å, $b = 63.1$ Å, $c = 31.6$ Å, $\beta = 110.7°$ and contain one Trx f per asymmetric unit. A 1.8 Å dataset, collected by Génovésio-Taverne (Génovésio-Taverne *et al.*, 1991) (Table 1) on an Enraf-Nonius FAST area detector diffractometer and processed with MADNES (Messerschmidt & Pflugrath, 1987) was used for molecular replacement. A conventional AMORE procedure was carried out, with integration radius 15 Å. The rotation and translation steps were performed between 8 and 3 Å and the final rigid-body fitting between 8 and 1.85 Å. The refinement, with X-PLOR, started with a new bulk-solvent correction calculation and an anisotropic refinement for the overall *B*-factor. A round of torsion angle simulated annealing was then performed with data up to the maximum resolution and was followed by positional and individual *B*-factor optimization. Manual rebuilding was then alternated with further cycles of bulk-solvent correction calculation, low-temperature simulated annealing and positional and thermal refinement. No sigma cut-off was used. Water molecules were added at positions where there was clear electron density in $F_o - F_c$ maps (peaks

higher than 3.5σ), provided that the environment allowed reasonable hydrogen bonding to the protein or to other water molecules.

Thioredoxin m

Crystallization

Trx m was crystallized *via* the hanging drop vapor diffusion method. A 2 ml sample of protein stock solution (50 mg/ml Trx m, 50 mM Tris-HCl (pH 7.3), 0.02 % (w/v) NaN_3) was mixed with an equal volume of reservoir solution containing 0.2 M $(NH_4)_2SO_4$, 0.1 M sodium acetate (pH 4.6), 30 % (w/v) PEG monomethylether 2000. All experiments were performed at 20 °C. This procedure yielded crystals of X-ray quality in about two weeks.

Data collection and space group determination

Data were collected at 4 °C, exactly as described above for Trx f. The space group of the crystals is $P3_121$ with cell dimensions $a = b = 74.7$ Å, $c = 74.0$ Å. The presence of the 3-fold screw axis was detected by inspection of the systematic absent reflections. The data were reduced with DENZO and SCALEPACK (Otwinowski & Minor, 1996). The statistics are given in Table 3.

Structure solution

Molecular replacement attempts were carried out with the program AMORE. A search model based on the refined coordinates of *E. coli* thioredoxin (with the non-conserved residues trimmed to alanine) could be easily positioned in the asymmetric unit. Two solutions were found, corresponding to the non-crystallographic dimer. The initial phases from these two models (*R*-factor 40.9 %) were improved by density modification methods (solvent flattening, histogram matching and twofold averaging with DM), which brought the DM *R*-free factor from 43 % down to 30 %. The resulting Fourier map was of very high quality: a model of Trx m encompassing residues 9-112 could be quickly built.

Structure refinement

The model was refined with X-PLOR against the native data, after 3.8 % of the reflections had been randomly selected and separated as a *R*-free test set. A first round of torsion angle simulated annealing with NCS constraints at 2.8 Å was followed by cycles of positional and *B*-factor refinement at increasing resolution (2.8 Å, 2.5 Å and 2.1 Å). The NCS constraints were replaced by NCS-restraints while extending the resolution from 2.8 to 2.5 Å. An overall temperature factor was used at 2.8 Å, grouped *B*-factors (two per residue) at 2.5 Å and finally individual *B*-factors at the maximum resolution. In the last 2.1 Å cycle the NCS restraints were released, resulting in a marked parallel decrease of the *R* and *R*-free factors. This last cycle was performed with the program CNS (Brünger *et al.*, 1998). In other respects the refinement was carried out as described for Trx f.

Preparation and data collection of reduced crystals

Native Trx m crystals were soaked in a stabilizing solution containing 0.2 M $(NH_4)_2SO_4$, 0.1 M sodium acetate (pH 4.6), 32 % (w/v) PEG monomethylether 2000 and 20 μM DTT. The DTT concentration was increased stepwise to 9 mM over a period of 28 hours. During this treatment the crystals were showing signs of stress, but at the end they still retained birefringence under polarized light. It was possible to collect a 2.3 Å complete and redundant data set from one of these (data collection conditions as for Trx f). The overall oscillation range was 110 °, corresponding to 53 hours data collection time.

Processing and splitting of the dataset of the reduced form of Trx m

In order to detect possible time-dependent changes in the reduced Trx m structure, the overall dataset corresponding to 110 ° and 53 hours was separated (with SCALEPACK) into an initial and a final dataset, each retaining an acceptable completeness (around 94 %). The two datasets were separated by a "blank" interval of 11 °, corresponding to approximately five hours. The statistics are given in Table 3.

Refinement of the initial and final reduced forms of Trx m

The reduced form of Trx m was refined, using X-PLOR, against the initial and final datasets, starting from the final oxidized Trx m structure. These two refinements were carried out in parallel, always following the same procedure, in order to allow a detailed comparison of the initial and of the final structure. The *R*-free factor selection of the oxidized Trx m was retained. The covalent bond constraint of the disulfide was removed and the van der Waals interactions between the sulfur atoms of the active site cysteine residues were made to be ignored, while the interaction potentials between each sulfur atom and the rest of the protein were retained. The model of oxidized Trx m first underwent torsion angle simulated annealing, followed by positional and individual *B*-factor refinement cycles, alternated with manual rebuilding. Water molecules which were not showing significant density due to the lower resolution were removed from the model. All other aspects of the two parallel refinements were handled as described for oxidized Trx m.

Data Bank accession numbers

The atomic coordinates and structure factors for the Trx f and Trx m structures have been deposited with the RCSB Protein Data Bank, with entry codes 1F9M, 1FAA, 1FB6 and 1FB0.

Acknowledgments

The authors thank Jean-Claude Génovésio-Taverne for collecting the Trx f-L dataset. G.C. is grateful to Professor W.R. Montfort for useful discussions and thanks Professor Markus G. Grütter and the Baugarten Foundation. This research was supported by Swiss National Science Foundation grant numbers 31-25712.88 and 31-36432.92 to J.N.J and 31-37725.93 and 31-47107.96 to P.S.

References

Aguilar, F., Brunner, B., Gardet-Salvi, L., Stutz, E. & Schürmann, P. (1992). Biosynthesis of active spinach-chloroplast thioredoxin f in transformed *E. coli*. *Plant Mol. Biol.* **20**, 301-306.

Andersen, J. F., Sanders, D. A., Gasdaska, J. R., Weichsel, A., Powis, G. & Montfort, W. R. (1997). Human thioredoxin homodimers: regulation by pH, role of aspartate 60, and crystal structure of the aspartate 60 → asparagine mutant. *Biochemistry*, **36**, 13979-13988.

Bairoch, A. & Apweiler, R. (1997). The SWISS-PROT protein sequence data bank and its supplement TrEMBL. *Nucl. Acids Res.* **25**, 31-36.

Barton, G. J. (1993). ALSCRIPT: a tool to format multiple sequence alignments. *Protein Eng.* **6**, 37-40.

Brandes, H. K., Larimer, F. W., Geck, M. K., Stringer, C. D., Schürmann, P. & Hartman, F. C. (1993). Direct identification of the primary nucleophile of thioredoxin f. *J. Biol. Chem.* **268**, 18411-18414.

Braun, H., Lichter, A. & Haberlein, I. (1996). Kinetic evidence for protein complexes between thioredoxin and NADP-malate dehydrogenase and presence of a thioredoxin binding site at the N terminus of the enzyme. *Eur. J. Biochem.* **240**, 781-788.

Brünger, A. T. (1992). Free *R* value: a novel statistical quantity for assessing the accuracy of crystal structures. *Nature*, **355**, 472-475.

Brünger, A. T., Adams, P. D., Clore, G. M., DeLano, W. L., Gros, P., Grosse-Kunstleve, R. W., Jiang, J. S., Kuszewski, J., Nilges, M., Pannu, N. S., Read, R. J., Rice, L. M., Simonson, T. & Warren, G. L. (1998). Crystallography & NMR system: a new software suite for macromolecular structure determination. *Acta Crystallog. sect. D*, **54**, 905-921.

Buchanan, B. B., Schürmann, P., Decottignies, P. & Lozano, R. M. (1994). Thioredoxin: a multifunctional regulatory protein with a bright future in technology and medicine. *Arch. Biochem. Biophys.* **314**, 257-260.

Chiadmi, M., Navaza, A., Miginiac-Maslow, M., Jacquot, J. P. & Cherfils, J. (1999). Redox signalling in the chloroplast: structure of oxidized pea fructose-1,6-bisphosphate phosphatase. *EMBO J.* **18**, 6809-6815.

Chivers, P. T. & Raines, R. T. (1997). General acid/base catalysis in the active site of *Escherichia coli* thioredoxin. *Biochemistry*, **36**, 15810-15816.

Chivers, P. T., Prehoda, K. E., Volkman, B. F., Kim, B. M., Markley, J. L. & Raines, R. T. (1997). Microscopic pKa values of *Escherichia coli* thioredoxin. *Biochemistry*, **36**, 14985-14991.

Collaborative Computational Project Number 4 (1994). The CCP4 suite: programs for protein crystallography. *Acta Crystallog. sect. D*, **50**, 760-763.

Danon, A. & Mayfield, S. P. (1994). Light-regulated translation of chloroplast messenger RNAs through redox potential. *Science*, **266**, 1717-1719.

de Lamotte-Guéry, F., Miginiac-Maslow, M., Decottignies, P., Stein, M., Minard, P. & Jacquot, J. P. (1991). Mutation of a negatively charged amino acid in thioredoxin modifies its reactivity with chloroplastic enzymes. In *Eur. J. Biochem.*, **196**, pp. 287-294, (published erratum appears in *Eur. J. Biochem.* (1991) **199**, 769).

De Lorimier, R., Hellinga, H. W. & Spicer, L. D. (1996). NMR studies of structure, hydrogen exchange, and main-chain dynamics in a disrupted-core mutant of thioredoxin. *Protein Sci.* **5**, 2552-2565.

DelVal, G., Maurer, F., Stutz, E. & Schürmann, P. (1999). Modification of the reactivity of spinach chloroplast thioredoxin *f* by site-directed mutagenesis. *Plant Sci.* **149**, 183-190.

Eklund, H., Gleason, F. K. & Holmgren, A. (1991). Structural and functional relations among thioredoxins of different species. *Proteins: Struct. Funct. Genet.* **11**, 13-28.

Forman-Kay, J. D., Clore, G. M., Wingfield, P. T. & Gronenborn, A. M. (1991). High-resolution three-dimensional structure of reduced recombinant human thioredoxin in solution. *Biochemistry*, **30**, 2685-2698.

Furey, W. (1989). *PHASES. Biocrystallography Laboratory*, VA Medical Center, Pittsburgh, USA.

Geck, M. K., Larimer, F. W. & Hartman, F. C. (1996). Identification of residues of spinach thioredoxin f that influence interactions with target enzymes. *J. Biol. Chem.* **271**, 24736-24740.

Génovésio-Taverne, J.-C., Jetzer, Y., Sauder, U., Hohenester, E., Huguet, C., Jansonius, J. N., Gardet-Salvi, L. & Schürmann, P. (1991). Crystallization and preliminary X-ray diffraction studies of the spinach-chloroplast thioredoxin f. *J. Mol. Biol.* **222**, 459-461.

Gronenborn, A. M., Clore, G. M., Louis, J. M. & Wingfield, P. T. (1999). Is human thioredoxin monomeric or dimeric? *Protein Sci.* **8**, 426-429.

Häberlein, I. & Vogeler, B. (1995). Completion of the thioredoxin reaction mechanism: kinetic evidence for protein complexes between thioredoxin and fructose 1,6-bisphosphatase. *Biochim. Biophys. Acta*, **1253**, 169-174.

Hartman, H., Syvanen, M. & Buchanan, B. B. (1990). Contrasting evolutionary histories of chloroplast thioredoxins f and m. *Mol. Biol. Evol.* **7**, 247-254.

Hirasawa, M., Schürmann, P., Jacquot, J. P., Manieri, W., Jacquot, P., Keryer, E., Hartman, F. C. & Knaff, D. B. (1999). Oxidation-reduction properties of chloroplast thioredoxins, ferredoxin:thioredoxin reductase, and thioredoxin f-regulated enzymes. *Biochemistry*, **38**, 5200-5205.

Hodges, M., Miginiac-Maslow, M., Decottignies, P., Jacquot, J.-P., Stein, M., Lepiniec, L., Crétin, C. & Gadal, P. (1994). Purification and characterization of pea thioredoxin f expressed in *Escherichia coli*. *Plant Mol. Biol.* **26**, 225-234.

Hol, W. G. (1985). Effects of the alpha-helix dipole upon the functioning and structure of proteins and peptides. *Adv. Biophys.* **19**, 133-165.

Holm, L. & Sander, C. (1993). Protein structure comparison by alignment of distance matrices. *J. Mol. Biol.* **233**, 123-138.

Holmgren, A. (1989). Thioredoxin and glutaredoxin systems. *J. Biol. Chem.* **264**, 13963-13966.

Holmgren, A. (1995). Thioredoxin structure and mechanism: conformational changes on oxidation of the active-site sulfhydryls to a disulfide. *Structure*, **3**, 239-243.

Holmgren, A., Söderberg, B. O., Eklund, H. & Brändén, C. I. (1975). Three-dimensional structure of *Escherichia coli* thioredoxin-S2 to 2.8 Å resolution. *Proc. Natl Acad. Sci. USA*, **72**, 2305-2309.

Honig, B. & Nicholls, A. (1995). Classical electrostatics in biology and chemistry. *Science*, **268**, 1144-1149.

Hooft, R. W., Vriend, G., Sander, C. & Abola, E. E. (1997). Errors in protein structures. *Nature*, **381**, 272.

Hutchinson, E. G. & Thornton, J. M. (1996). PROMOTIF–a program to identify and analyze structural motifs in proteins. *Protein Sci.* **5**, 212-220.

Jacquot, J.-P., Lancelin, J.-M. & Meyer, Y. (1997). Thioredoxins: structure and function in plant cells. *New Phytol.* **136**, 543-570.

Janin, J. (1997). Specific versus non-specific contacts in protein crystals. *Nature Struct. Biol.* **4**, 973-974.

Jeng, M.-F. & Dyson, H. J. (1994). High-resolution solution structures of oxidized and reduced *Escherichia coli* thioredoxin. *Structure,* **2**, 853-868.

Jones, T. A. & Kjeldgaard, M. (1991). Manual for O, 5.6 edit, Uppsala University, Uppsala, Sweden.

Katti, S. K., LeMaster, D. M. & Eklund, H. (1990). Crystal structure of thioredoxin from *Escherichia coli* at 1.68 Å resolution. *J. Mol. Biol.* **212**, 167-184.

Kortemme, T., Darby, N. J. & Creighton, T. E. (1996). Electrostatic interactions in the active site of the N-terminal thioredoxin-like domain of protein disulfide isomerase. *Biochemistry,* **35**, 14503-14511.

Kraulis, P. J. (1991). MOLSCRIPT: a program to produce both detailed and schematic plots of protein structures. *J. Appl. Crystallog.* **24**, 946-950.

Laskowski, R. A., MacArthur, M. W., Moss, D. S. & Thornton, J. M. (1993). PROCHECK: a program to check the stereochemical quality of protein structure. *J. Appl. Crystallog.* **26**, 283-291.

LeMaster, D. M. (1996). Structural determinants of the catalytic reactivity of the buried cysteine of *Escherichia coli* thioredoxin. *Biochemistry,* **35**, 14876-14881.

LeMaster, D. M., Springer, P. A. & Unkefer, C. J. (1997). The role of the buried aspartate of *Escherichia coli* thioredoxin in the activation of the mixed disulfide intermediate. *J. Biol. Chem.* **272**, 29998-30001.

Levings, C. S., III & Siedow, J. N. (1995). Regulation by redox poise in chloroplasts. *Science,* **268**, 695-696.

Livingstone, C. D. & Barton, G. J. (1993). Protein sequence alignments: a strategy for the hierarchical analysis of residue conservation. *Comput. Appl. Biosci.* **9**, 745-756.

Marcus, F., Moberly, L. & Latshaw, S. P. (1988). Comparative amino acid sequence of fructose-1,6-bisphosphatases: identification of a region unique to the light-regulated chloroplast enzyme. *Proc. Natl Acad. Sci. USA,* **85**, 5379-5383.

Messerschmidt, A. & Pflugrath, J. W. (1987). Crystal orientation and X-ray pattern prediction routines for area-detector diffractometer systems in macromolecular crystallography. *J. Appl. Crystallog.* **20**, 306-315.

Mittard, V., Blackledge, M. J., Stein, M., Jacquot, J. P., Marion, D. & Lancelin, J. M. (1997). NMR solution structure of an oxidised thioredoxin h from the eukaryotic green alga *Chlamydomonas reinhardtii*. *Eur. J. Biochem.* **243**, 374-383.

Mora-García, S., Rodríguez-Suárez, R. & Wolusiuk, R. A. (1996). Role of electrostatic interactions on the affinity of thioredoxin for target proteins. *J. Biol. Chem.* **273**, 16273-16280.

Nicastro, G., De Chiara, C., Pedone, E., Tato, M., Rossi, M. & Bartolucci, S. (2000). NMR solution structure of a novel thioredoxin from bacillus acidocaldarius possible determinants of protein stability (in process citation). *Eur. J. Biochem.* **267**, 403-413.

Nikkola, M., Gleason, F. K., Fuchs, J. A. & Eklund, H. (1993). Crystal structure analysis of a mutant *Escherichia coli* thioredoxin in which lysine 36 is replaced by glutamic acid. *Biochemistry,* **32**, 5093-5098.

Nishizawa, A. N. & Buchanan, B. B. (1981). Enzyme regulation in C4 photosynthesis. Purification and properties of thioredoxin-linked fructose bisphosphatase and sedoheptulose bisphosphatase from corn leaves. *J. Biol. Chem.* **256**, 6119-6126.

Otwinowski, Z. & Minor, W. (1996). Processing of X-ray diffraction data collected in oscillation mode. In *Methods in Enzymology* (Carter, C. W. & Sweet, R. M., eds), vol. 276, Academic Press, New York.

Philippsen, A. (1998). DINO, *a visualization system for structural data.* http//www.bioz.unibas.ch/ ~ xray/dino.

Pla, A. & Lopez-Gorge, J. (1981). Thioredoxin/fructose-1,6-bisphosphatase affinity in the enzyme activation by the ferredoxin-thioredoxin system. *Biochim. Biophys. Acta,* **636**, 113-118.

Qin, J., Clore, G. M., Poindexter Kennedy, W. M., Huth, J. R. & Gronenborn, A. M. (1995). Solution structure of human thioredoxin in a mixed disulfide intermediate complex with its target peptide from the transcription factor NFkappaB. *Structure,* **3**, 289-297.

Qin, J., Clore, G. M., Kennedy, W. P., Kuszewski, J. & Gronenborn, A. M. (1996). The solution structure of human thioredoxin complexed with its target from Ref-1 reveals peptide chain reversal. *Structure,* **4**, 613-620.

Saarinen, M., Gleason, F. K. & Eklund, H. (1995). Crystal structure of thioredoxin-2 from *Anabaena. Structure,* **3**, 1097-1108.

Sahrawy, M., Hecht, V., Lopez-Jaramillo, J., Chueca, A., Chartier, Y. & Meyer, Y. (1996). Intron position as an evolutionary marker of thioredoxins and thioredoxin domains. *J. Mol. Evol.* **42**, 422-431.

Sahrawy, M., Chueca, A., Hermoso, R., Lázaro, J. J. & Gorgé, J. L. (1997). Directed mutagenesis shows that the preceding region of the chloroplast fructose-1,6-bisphosphatase regulatory sequence is the thioredoxin docking site. *J. Mol. Biol.* **269**, 623-630.

Salamon, Z., Gleason, F. K. & Tollin, G. (1992). Direct electrochemistry of thioredoxins and glutathione at a lipid bilayer-modified electrode. *Arch. Biochem. Biophys.* **299**, 193-198.

Sanner, M. F., Olson, A. J. & Spehner, J. C. (1996). Reduced surface: an efficient way to compute molecular surfaces. *Biopolymers,* **38**, 305-320.

Schürmann, P. (1995). The ferredoxin/thioredoxin system. *Methods Enzymol.* **252**, 274-283.

Schwarz, O., Schürmann, P. & Strotmann, H. (1997). Kinetics and thioredoxin specificity of thiol modulation of the chloroplast H + -ATPase. *J. Biol. Chem.* **272**, 16924-16927.

Soulié, J. M., Buc, J., Rivière, M. & Ricard, J. (1985). Equilibrium binding of thioredoxin fb to chloroplastic fructose bisphosphatase. Evidence for a thioredoxin site distinct from the active site. *Eur. J. Biochem.* **152**, 565-568.

Tsugita, A., Maeda, K. & Schürmann, P. (1983). Spinach chloroplast thioredoxins in evolutionary drift. *Biochem. Biophys. Res. Commun.* **115**, 1-7.

Villeret, V., Huang, S., Zhang, Y., Xue, Y. & Lipscomb, W. N. (1995). Crystal structure of spinach chloroplast fructose-1,6-bisphosphatase at 2.8 Å resolution. *Biochemistry,* **34**, 4299-4306.

Vohnik, S., Hanson, C., Tuma, R., Fuchs, J. A., Woodward, C. & Thomas, G. J., Jr (1998). Conformation, stability, and active-site cysteine titrations of *Escherichia coli* D26A thioredoxin probed by Raman spectroscopy. *Protein Sci.* **7**, 193-200.

Weichsel, A., Gasdaska, J. R., Powis, G. & Montfort, W. R. (1996). Crystal structures of reduced, oxidized, and mutated human thioredoxins: evidence for a regulatory homodimer. *Structure,* **4**, 735-751.

Wenderoth, I., Scheibe, R. & von Schaewen, A. (1997). Identification of the cysteine residues involved in redox modification of plant plastidic glucose-6-phosphate dehydrogenase. *J. Biol. Chem.* **272**, 26985-26990.